Korean J. Chem. Eng., 37(2), 263-273 (2020)
DOI: 10.1007/s11814-019-0441-5

pISSN: 0256-1115
eISSN: 1975-7220

Glycidyl POSS-functionalized ZnO nanoparticles incorporated polyether-imide based nanofiltration membranes for heavy metal ions removal from water

Samaneh Bandehali*, Abdolreza Moghadassi*,†, Fahime Parvizian*, Jiangnan Shen, and Sayed Mohsen Hosseini*,†**

*Department of Chemical Engineering, Faculty of Engineering, Arak University, Arak 38156-8-8349, Iran
**Center for Membrane Separation and Water Science & Technology, Ocean College,
Zhejiang University of Technology, Hangzhou 310014, China
(*Received 7 September 2019 • accepted 24 November 2019*)

Abstract−Surface functionalization of zinc oxide (ZnO) nanoparticles was performed by glycidyl POSS. The synthesized nanoparticles were applied to prepare polyether-imide based-nanofiltration membranes by phase inversion method. The characterizations were done by FESEM, EDX and AFM analysis. The effect of different concentrations of POSS-ZnO (PZ) nanoparticles was investigated to evaluate the separation performance of prepared membranes by contact angle measurement, pure water flux (PWF), rejection of aqueous solutions including Na_2SO_4, $Pb(NO_3)_2$, $Cu(NO_3)_2$ and flux recovery ratio (FRR%). The prepared PEI/PZ membranes showed significant separation performance and antifouling properties compared with neat PEI and PEI/ZnO membranes. The highest pure water flux (42.4 L/m^2h) was revealed for M1-PZ in 0.001 wt% of PZ nanoparticles, whereas that was 17 (L/m^2h) for neat membrane and 12-18 (L/m^2h) for PEI/ZnO, respectively. Also, salt rejection was low for blended PEI/ZnO membranes. By incorporation of PZ into the PEI, Na_2SO_4, and Pb $(NO_3)_2$ rejection improved to 83% and 59%, respectively. Moreover, the M3-PZ showed the best separation performance for Cu $(NO_3)_2$ with the rejection of 67%. The highest antifouling properties were obtained for M4-PZ with FRR% of 59%, which is significant compared with 15% for PEI/ZnO and 30% for neat PEI membranes.

Keywords: Nanofiltration, Zinc Oxide Nanoparticles, Glycidyl POSS-functionalized ZnO, Outstanding Separation Performance, Heavy Metal Removal

INTRODUCTION

Membrane filtration, such as ultrafiltration (UF), microfiltration (MF), nanofiltration (NF), reverse osmosis (RO) and electrodialysis (ED), is an environmentally friendly, highly efficient technology for water purification [1,2]. NF, as a major membrane process was introduced in the 1980s and is operated in the range of 1-20 bar, including pore sizes of 1 nm [3,4]. One of the greatest challenges in NF membranes is fouling, which significantly reduces their separation performance. Fouling increases the consumption of energy and the operating costs. The methods for fouling control are followed by the improvement of membrane hydrophilicity and decreased surface roughness of membranes. For this purpose, surface modification, including physical and chemical modification, grafting, adsorption, and blending, has been applied [5-7]. Among these modifications, blending with hydrophilic additives, including organic and inorganic materials, have been used extensively [8-11]. Organic and inorganic nanomaterials such as titanium dioxide, iron oxide, graphene oxide, carbon nanotubes, chitosan, and cellulose acetate have been used for decreasing membrane fouling and enhancement of chemical resistance and mechanical strength without decreasing salt rejection. But the application of inorganic nanomaterials for the fabrication of membranes leads to agglomeration and bad dispersion of nanoparticles. The methods for overcoming this are nanoparticle functionalization with desirable groups and preparation of new composite nanoparticles [12,13]. In this study, the functionalization of ZnO nanoparticles was considered by glycidyl-POSS. Zinc oxide (ZnO) nanoparticles with advantages such as high surface area, suitable non-toxic, low cost, high thermal and chemical stability, good antibacterial properties are attractive in membrane applications [14,15]. The application of ZnO nanoparticles into the membrane matrix increases the stability of a system at the operating condition. Moreover, the physical and chemical properties of membrane improve and that leads to the improvement of the anti-fouling properties of prepared membranes [12]. Rajabi et al. [16] synthesized ZnO nanoparticles and ZnO nanorods for preparation of PES-based membranes. The prepared membranes showed high-water permeability, high resistance of fouling in 0.1 wt% ZnO nanoparticles. Moreover, membrane durability improved, and ZnO nanorods showed higher performance than ZnO nanoparticles. Zinadini et al. [12] applied the coated multiwalled carbon nanotubes (MWCNTs) by ZnO for the fabrication of PES membranes. These nanoparticles significantly increased the water permeability. The application 0.5 wt% ZnO/MWCNTs into the PES membrane showed the best anti-fouling properties of prepared membranes. Moreover, the results exhibited good Direct Red 16 rejection.

Polyhedral oligomeric silsesquioxane (POSS) as organic and inorganic nanomaterial is attractive due to high functional groups in its structure. POSS with its cage structure in combination with poly-

†To whom correspondence should be addressed.
E-mail: a-moghadassi@araku.ac.ir, s-hosseini@araku.ac.ir

mers increases rigidity and adsorption capacity of pollutants. The presence of functional groups increases affinity with organic and inorganic materials. The reactive functional groups of POSS lead to reactions of cross-linking in solutions and thus create strengthened physicochemical characteristics. The size of POSS molecules is in the range of 1-3 nm. POSS nanomaterials show high dispersity into the common solvents [17-20]. Therefore, in this work, POSS with its special properties was applied to functionalization of ZnO nanoparticles. Studies showed a high potential of POSS materials for enhancement of membrane performance in wastewater treatment. You et al. [21] used POSS nanoparticles for tuning pores in polydopamine (PDA) membrane by a facile co-deposition process on polyacrylonitrile (PAN) substrate. The prepared membranes showed high porosity with narrow nanopore size in about 1.04-1.07 nm. The high porosity of fabricated membranes increased remarkably the water permeability and dye rejection. He et al. [18] showed the capacity of POSS nanomaterials for adsorption of arsenic and selenium by NF membranes. Moreover, the construction of thin-film nanocomposite membranes from different POSS nanomaterial such as P-8Phenyl, P-8NH_3Cl, P-8NH_2, and P-1NH_2 was investigated in desalination applications and wastewater treatment [17,19,22-24]. In this study, the functionalization of ZnO by glycidyl POSS was performed for the fabrication of PEI-based NF membranes for separation of Na_2SO_4, Pb $(NO_3)_2$ and Cu $(NO_3)_2$ salts. The epoxy groups in glycidyl POSS are unstable even in aqueous solution; therefore, it has high reactivity with hydroxyl groups in ZnO nanoparticles. Moreover, polyether-imide (PEI) exhibits high thermal and chemical stability, good mechanical strength with high ability in film forming [25-29]. Thus, it is expected that the presence of ZnO-POSS nanomaterials into the PEI membranes can improve porosity and water permeability, adsorption capacity and anti-fouling properties.

MATERIALS AND METHODS

1. Materials

Octaglycidyloxypropyl-silsesquioxane (Glycidyl-POSS) was purchased from Iran Polymer and Petrochemical Institute. Polyether-imide (PEI) (M_w: 35,000) was supplied from Sigma Aldrich. N, N-dimethylacetamide (DMAc) and tetrahydrofuran (THF) were purchased from DAEJUNG, Korea as a solvent. Zinc oxide nanoparticles and polyvinylpyrrolidone (PVP) as pore-forming were purchased from Merck. Aqueous solutions of Na_2SO_4, $Pb(NO_3)_2$ and $Cu(NO_3)_2$ were applied as feed solutions for studies of membrane separation.

2. Synthesis of Functionalized-zinc Oxide Nanoparticles

The preparation of functionalized-ZnO nanoparticles by glycidyl-POSS was followed by dispersion ZnO nanoparticles into THF and stirring for obtaining a homogeneous mixture. Then glycidyl-POSS was added to it. The solution was heated at 50 °C and stirring followed for 6 h. Then the prepared solution was kept at ambient temperature for 24 h. The glycidyl-POSS functionalized-ZnO (PZ) powder was dried in a vacuum oven at 50 °C for 14 h. Fig. 1 shows the synthesis route of PZ nanoparticles.

3. Membrane Preparation

PEI/PZ and PEI/ZnO membranes were fabricated by phase inversion method and immersion into the water bath. First, PEI

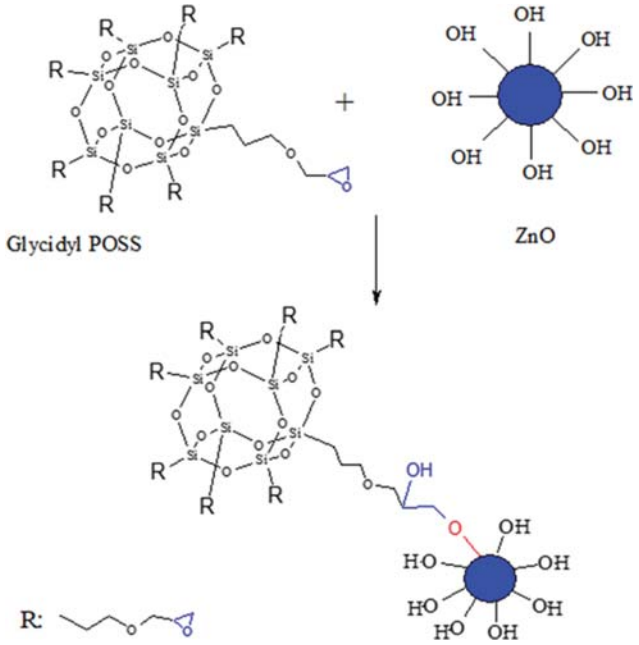

Fig. 1. The synthesis route for functionalization of ZnO by glycidyl POSS.

with 18 wt% and PVP at 1 wt% as a pore-forming agent was solved into the DMAc as a solvent. Then different concentrations of ZnO and PZ nanoparticles (0, 0.001, 0.01, 0.1 to 1 wt%) were added to the solution in the prior step and stirred for 20 h at 60 °C for obtaining a homogeneous solution. After that, the air bubbles from the fabricated solution were removed by keeping the solution at ambient temperature for 12 h. The NF membranes were constructed by spreading on a clean glass plate and an applicator. The membranes were soaked in deionized water for 24 h for the complete phase inversion process. The final thickness of prepared membranes was 120 μm. The prepared membranes were indicated as M1-ZnO, M2-ZnO, M3-ZnO, M4-ZnO with 0.001, 0.01, 0.1, 1 wt% of ZnO nanoparticles, and also, M1-PZ, M2-PZ, M3-PZ, M4-PZ are blended membranes containing of 0.001, 0.01, 0.1 and 1 wt% of (POSS-ZnO) PZ nanoparticles. The M0 was related to neat PEI-membrane. The composition of polymeric solution is summarized in Table 1.

4. Characterization Methods

4-1. Membrane and Nanoparticle Characterization

Fourier transform infrared spectroscopy (FTIR) was used to confirm fabrication synthesis of nanoparticles and their presence in the membranes. FTIR spectra were recorded with a Bruker spec-

Table 1. Details of compositions for the preparation of membranes

Membrane	PEI (wt%)	ZnO and POSS-ZnO	PVP (wt%)	DMAc (wt%)
M0	18	0	1	81%
M1	18	0.001%	1	80.999%
M2	18	0.01%	1	80.99%
M3	18	0.1%	1	80.9%
M4	18	1%	1	80

trometer (TENSOR 27) in the range of 500 to 4,000 cm^{-1} at resolution of 1 cm^{-1} for each spectrum. The energy dispersive X-ray (EDX) analytical method was applied to show the dispersion of nanoparticles into the membrane structure. The morphology of membranes and nanoparticles was examined by field emission scanning electron microscopy (FESEM). The roughness and surface morphology of fabricated membranes were determined by atomic force microscope (AFM) (FemtoScan model made in Russia) with scanning area 6 μm×6 μm.

4-2. Membrane Filtration Performance

The cross-flow nanofiltration system was used for the calculation of separation performance of fabricated membranes. Membrane testing was carried out at ambient temperature and 4.5 bar. Before the membrane testing, membrane compaction was done with deionized water for 30 min at 5 bar to obtain a steady state condition. Membrane rejection was determined by the aqueous solutions of Na_2SO_4 (1,100 mg/L), $Pb(NO_3)_2$, $Cu(NO_3)_2$ with concentration 500 mg/L. Membrane fouling was examined by flux recovery ratio (FRR%) by washing fouled membranes in deionized water and measurement of pure water flux (PWF) at 4.5 bar and room temperature.

Eqs. (1) and (2) were applied to measure membrane porosity and mean pore size of the prepared membrane [30-32]:

$$\varepsilon(\%) = \frac{(W_w - W_d)}{\rho_f V_m} \times 100 \quad (1)$$

$$r_m = \sqrt{\frac{(2.9 - 1.75\varepsilon) 8 \eta LQ}{\varepsilon A \Delta p}} \quad (2)$$

All calculations were repeated three times and the average values were reported for reducing experimental error, where W_d and W_w (g) are dry weight and wet weight of membrane respectively. ρ_f is water density (g/cm^3). V_m is volume (cm^3). η, Q, ΔP are the water viscosity (8.9×10^{-4} Pa·s), the volume of the permeated pure water flux (m^3/s) and operating pressure (0.45 MPa) respectively. A, ε and l are the membrane filtration area (m^2), porosity and the thickness of membranes (m). The contact angle of fabricated membranes was obtained by contact angle analyzer for determination of membrane hydrophilicity properties.

The pure water flux (PWF), salt rejection and FRR% of fabricated membranes were calculated by Eq. (3), (4) and Eq. (6) [4,25]:

$$J_{w,1} = \frac{V}{A \times t} \quad (3)$$

$$R(\%) = f\left(1 - \frac{C_p}{C_f}\right) \times 100 \quad (4)$$

$$FRR\% = \left(\frac{J_{w,2}}{J_{w,1}}\right) \times 100 \quad (5)$$

where $J_{w,1}$, V are the PWF ($Lm^{-2}h^{-1}$) and volume of solution in permeated water, A and t are the effective area of membrane (11.94 cm^2) and time (h). C_f and C_p are the feed and permeate concentration, respectively. $J_{w,2}$ (L/m^2h) is the PWF of fouled membranes after washing.

RESULTS AND DISCUSSION

1. Characterization of ZnO, PZ Nanoparticles and Prepared Membranes

The chemical structures of ZnO, and PZ nanoparticles were determined by FTIR analysis as shown in Fig. 2. The FTIR spectrum of ZnO and PZ nanoparticles are shown in the range of 500-4,000 cm^{-1}. The presence of hydroxyl groups was observed at 3,383 cm^{-1} [33,34]. The band 1,735 cm^{-1} is attributed to present carbonyl groups of imide rings [35]. The strong absorption bond around 1,101 cm^{-1} was attributed to the presence of Si-O-Si group in the PZ and PEI/PZ membranes [36,37]. Zn-O bonds were determined at the peak

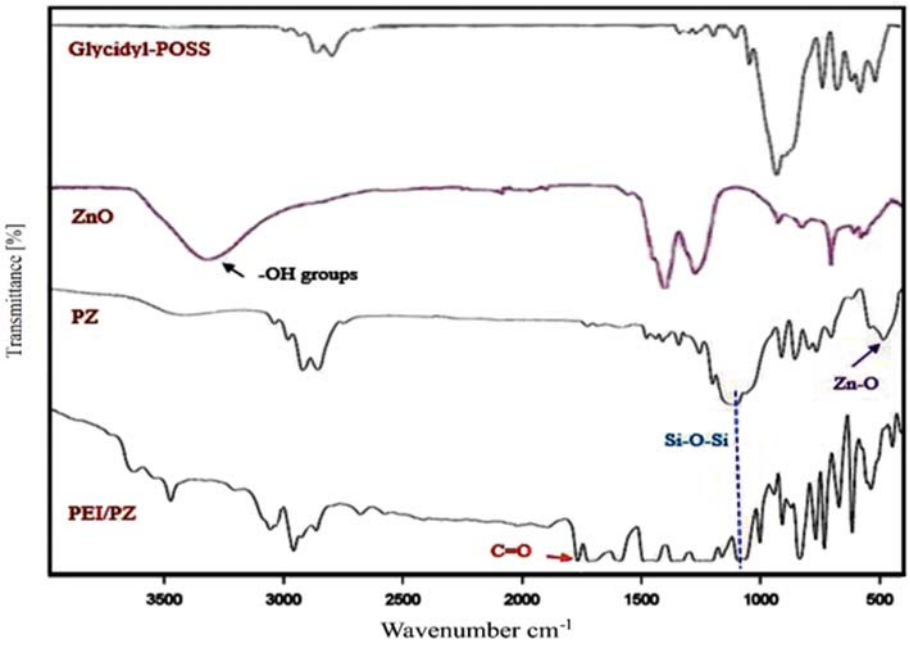

Fig. 2. The FTIR analysis of ZnO, PZ nanoparticles, glycidyl POSS and PEI/PZ (1 wt%) membranes.

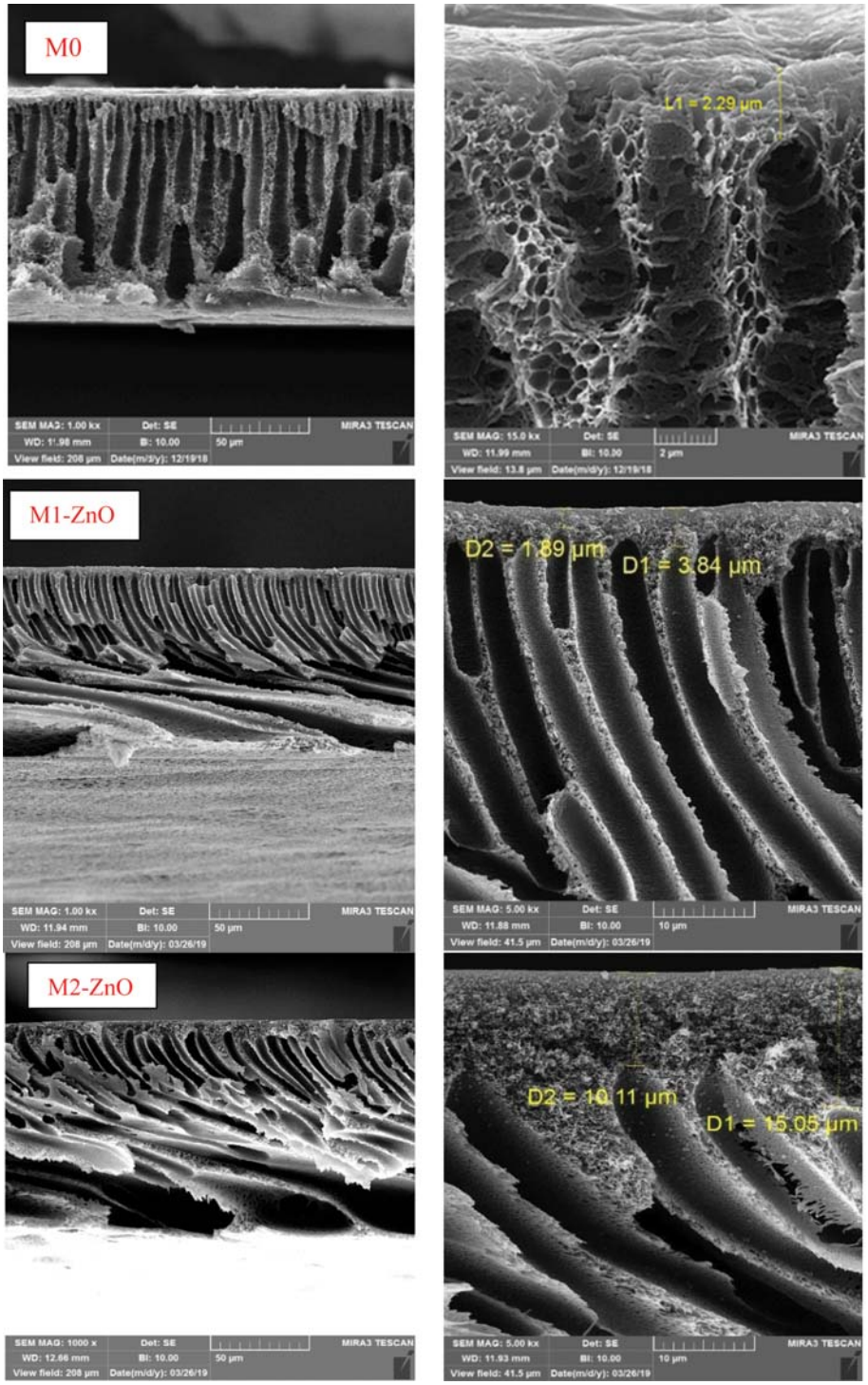

Fig. 3. FESEM images of the prepared membranes from ZnO nanoparticles and POSS-ZnO nanoparticles.

of 510 and 640 cm^{-1} [14].

2. Membrane Morphology

FESEM, EDX and AFM were applied to characterize the surface morphology of PEI/ZnO and PEI/PZ membranes. The FESEM cross-section images of all prepared membranes (PEI/ZnO and PEI/PZ) are shown in Fig. 3. The images of EDX and AFM are shown in Fig. 4 and Fig. 5. All prepared membranes show asymmetric structure, including a top layer as selective layer and a support layer with porous structure. The phase inversion process leads to exchange between solvent and non-solvent (deionized water) and produces a asymmetric structure. By increasing the nanoparticle loading, the thickness of selective layer changes and acts as a barrier layer and increases by incorporation of ZnO nanoparticles. The highest thickness of selective layer was observed for M2-ZnO

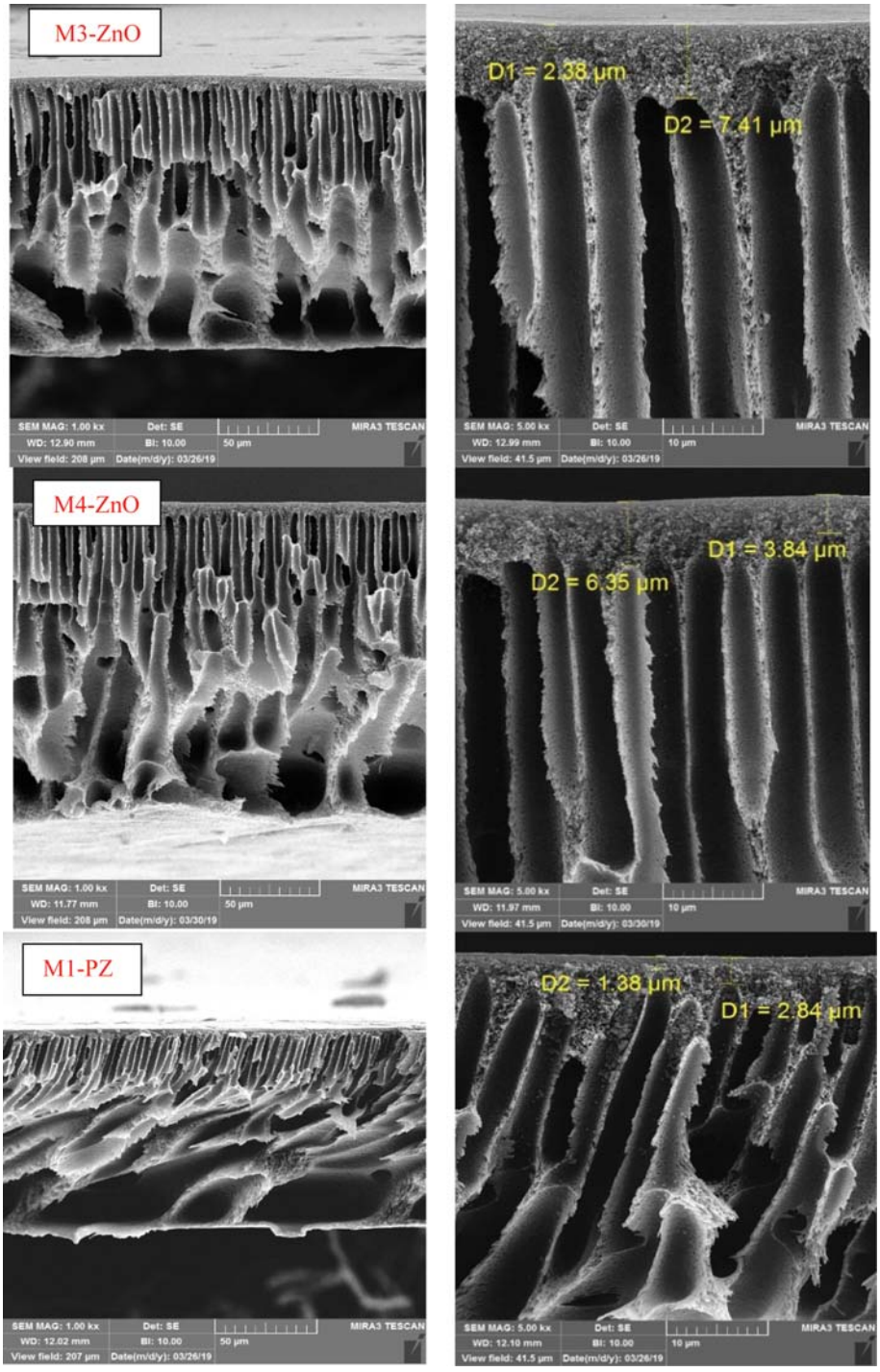

Fig. 3. Continued.

at 0.01 wt% of ZnO nanoparticles. Then the thickness of selective layer decreased in M3-ZnO and M4-ZnO. This decreasing can be explained due to ZnO nanoparticle agglomeration at high concentration [32,38]. Moreover, the thickness of selective layer of PEI/PZ membranes increased with increasing PZ nanoparticles. The highest thickness of selective layer was observed for M4-PZ. Longer and larger porosities were obtained for porous layer and increased in the high concentration of nanoparticles. Because by introducing nanoparticles, the interactions between polymer chains are reduced and the rate of exchange solvent and non-solvent increase due to hydrophilic properties of nanoparticles. These parameters lead to more and longer porosity [35,39,40]. The structure of PEI/ZnO and PEI/PZ membranes revealed better dispersion of PZ nanoparticles due to more interaction between PEI and PZ nanoparticles and creating hydrogen bonding between hydroxyl groups and carbonyl group of imide ring of PEI [41]. Functionalization of

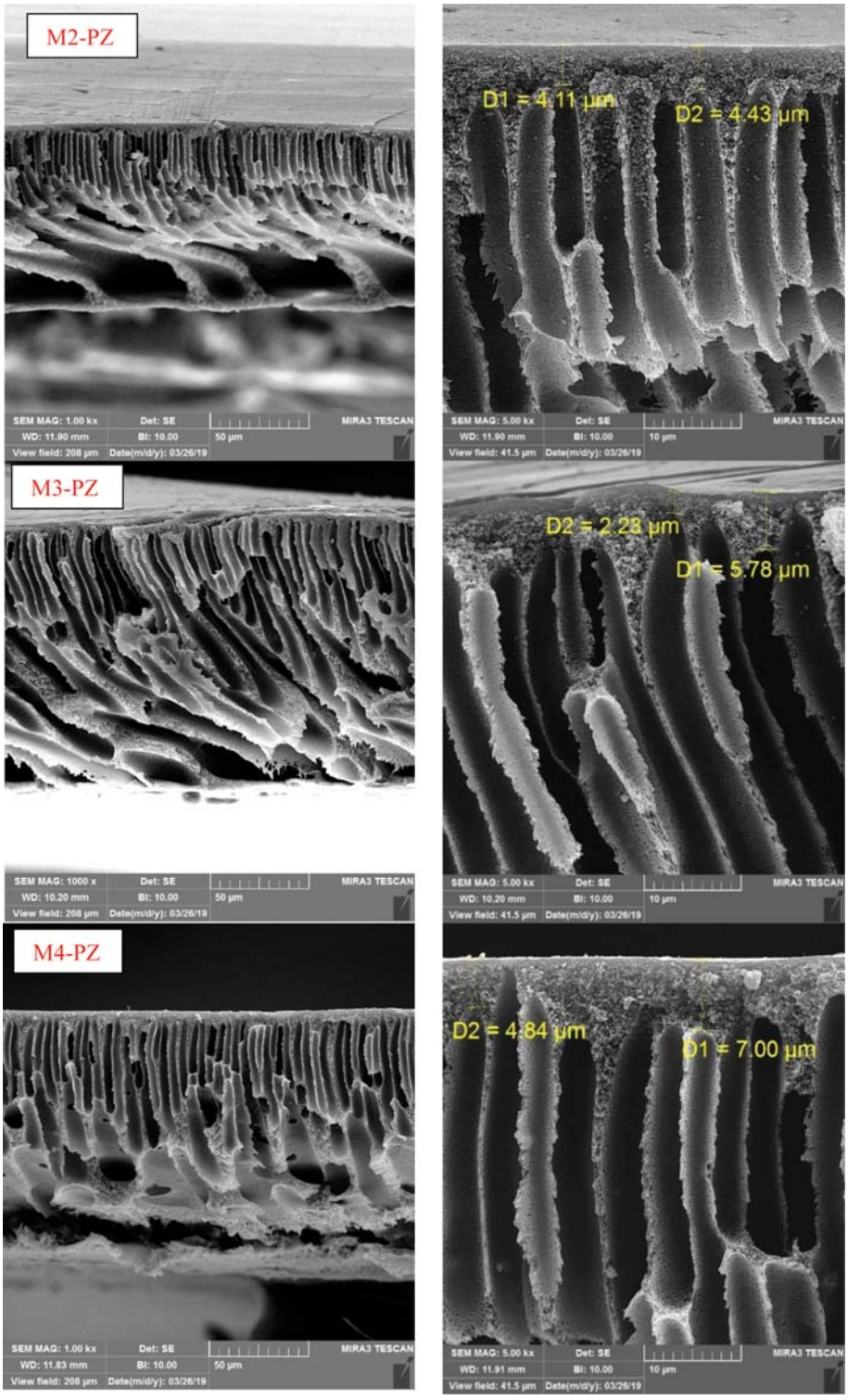

Fig. 3. Continued.

ZnO by POSS conveniently improves incorporation for the construction of composite polymers [42]. PZ nanoparticles show tuning porosities because of the cage and rigid structure of POSS [21]. Mapping and EDX analysis of M2-PZ was applied to confirm the uniform structure of nanoparticle dispersion and the presence of Si element of PZ nanoparticles (see Fig. 4).

The surface morphology of prepared membranes was evaluated by AFM analysis. The AFM image and the roughness parameters are shown in Fig. 5. The results show a smoother surface for PEI/PZ than PEI membranes. The average roughness (R_a) was reduced from 20.01 nm in pure PEI to 1.90 nm in M3-PZ. Thus, the incorporation of PZ nanoparticles led to better dispersion of PZ nanopar-

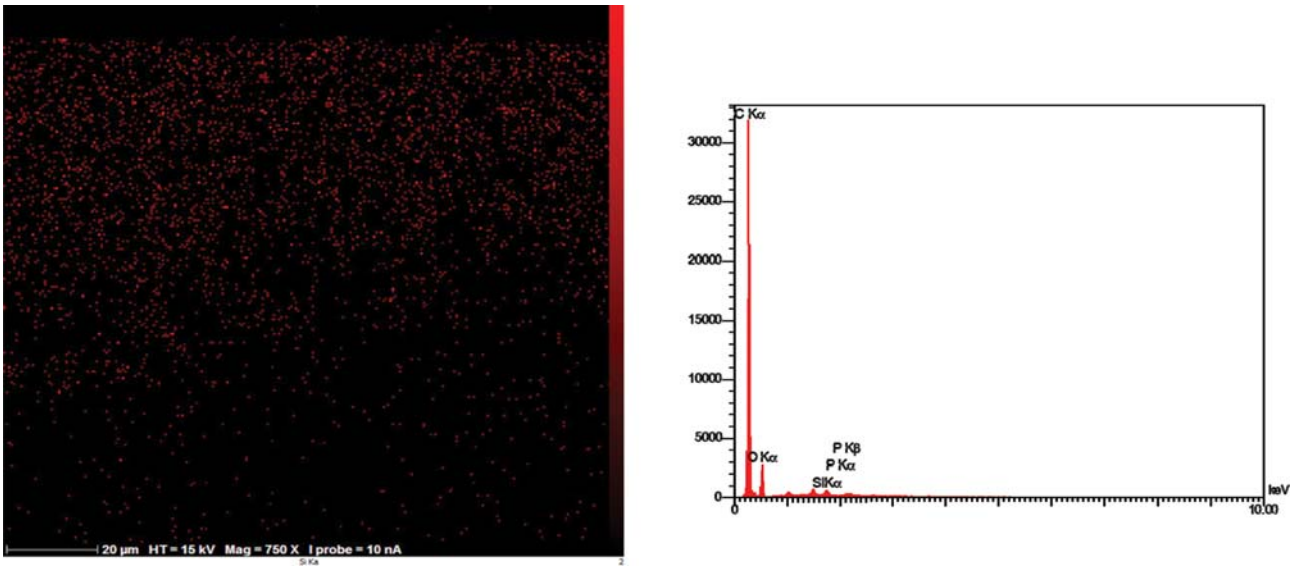

Fig. 4. EDX analysis of M2-PZ membrane.

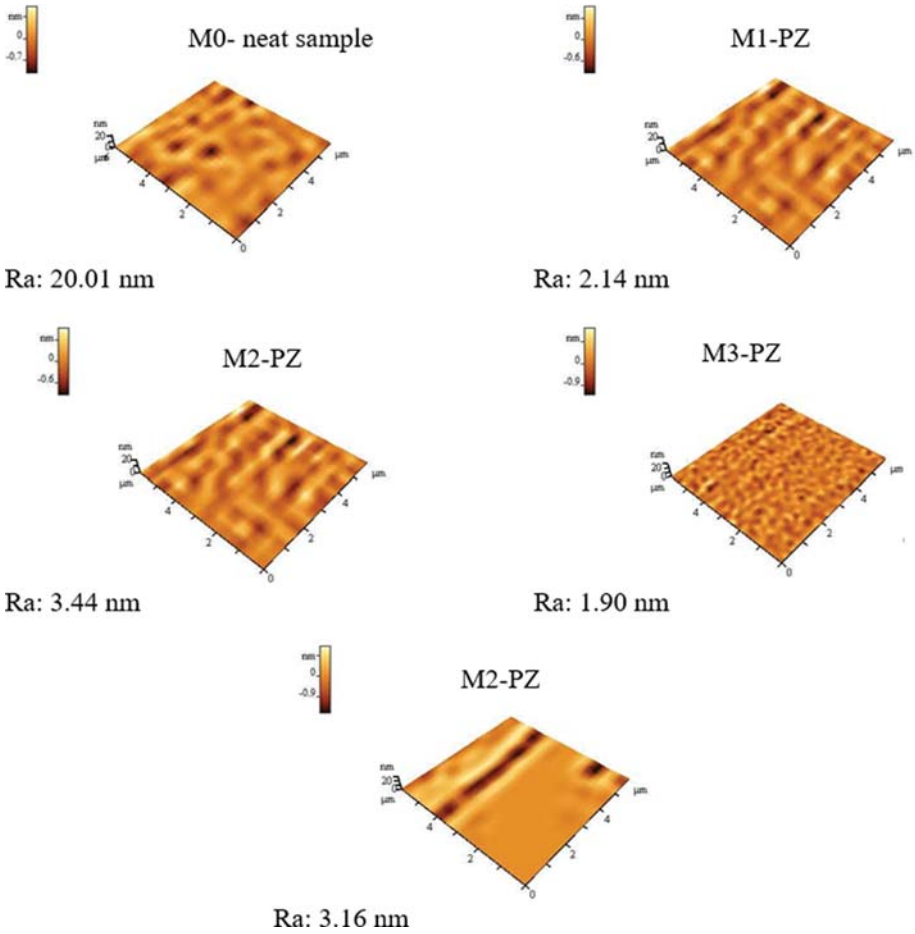

Fig. 5. AFM images of PEI/PZ membranes.

ticles into the membrane and a smoother surface.

3. Membrane Separation Performance

Membrane hydrophilicity, which is important in the separation process, is determined by the contact angle. Fig. 6 shows the change of contact angle in PEI/ZnO and PEI/PZ and pristine PEI membranes. Incorporation of ZnO and PZ nanoparticles decreased the

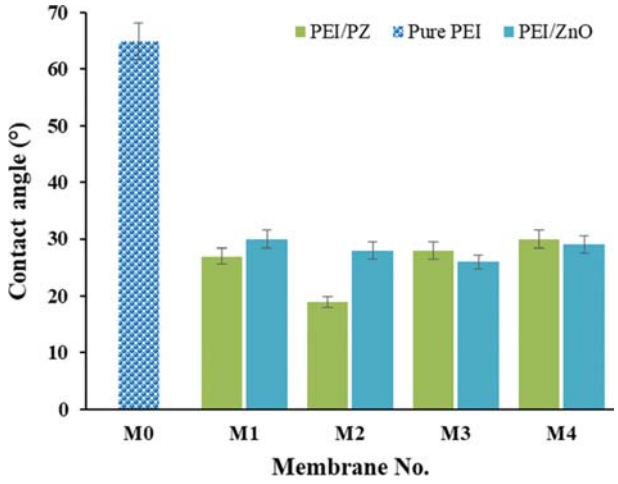

Fig. 6. Contact angle for the prepared membranes.

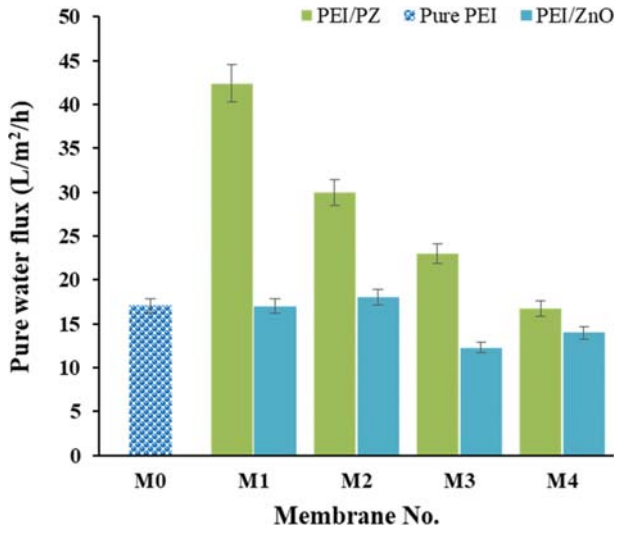

Fig. 7. Pure water flux for all prepared membranes.

contact angle of membranes from 65° to in the range of 20-30°, therefore improving membrane hydrophilicity due to hydrophilic groups such as hydroxyl. The result of pure water flux (PWF) is summarized in Fig. 7 for different concentrations of ZnO and PZ nanoparticles. Pure water flux of modified membranes by PZ nanoparticles improved compared with pristine membrane. But the significant increasing of PWF by PEI/ZnO membranes was not observed compared to the pristine membranes. The highest PWF in PEI/ZnO nanoparticles was obtained 18 (L/m^2h), which was fairly similar to other reported values by ZnO nanoparticles. While, the water permeability enhanced significantly in PEI/PZ nanoparticles and the highest PWF recorded 42.4 (L/m^2h) in M1-PZ and then decreased to 16.75 (L/m^2h) in M4-PZ by increasing nanoparticle concentration. It is often considered that strong interaction is created between water molecules and oxygen-containing groups in the POSS and ZnO structure [43-45]. Therefore, the free paths for water transport decreased by increasing PZ nanoparticles. As shown in Table 2, the porosity of membranes decreased in a high concentration of nanoparticles, and the highest porosity was observed in M1-PZ, which is in agreement with the results of PWF. Moreover, the cage structure of POSS affects the increasing free path for water molecule transport. Therefore, the functionalization of ZnO nanoparticles by glycidyl-POSS improved the PWF in ZnO-containing membranes.

Table 2. Membrane porosity and mean pore size for fabricated membranes

Sample	Porosity (%)	Mean pore size (nm)
M0	56.01	4.20
M1-PZ	75.11	1.89
M2-PZ	68.09	1.97
M3-PZ	62.03	1.87
M4-PZ	61.22	1.61
M1-ZnO	75.42	1.39
M2-ZnO	69.31	1.52
M3-ZnO	67.12	1.27
M4-ZnO	69.25	1.34

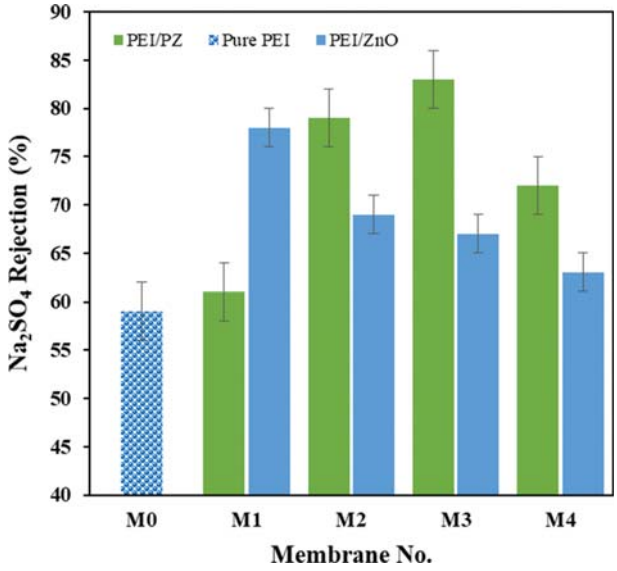

Fig. 8. The Na_2SO_4 rejection of pure PEI, PEI/ZnO and PEI/PZ membranes.

The separation performance of all prepared membranes was evaluated by the aqueous solution of Na_2SO_4 (1,000 mg/*l*). The result of salt rejection is shown in Fig. 8. As shown, the Na_2SO_4 rejection increased to 83% in M3-PZ in 0.1 wt% of PZ nanoparticles, which can be explained by Donnan exclusion mechanism and molecular sieve. The oxygen groups and hydroxyl groups with their negative charges on the nanoparticle surface repulse the SO_4^{2-} ions and that led to rejection of Na_2SO_4 salt. Moreover, the cage structure of POSS particles reduced surface pores and created narrow pores which lead to increase rejection [18,46].

The Na_2SO_4 rejection did not increase significantly by incorporation of ZnO nanoparticles, and the highest Na_2SO_4 rejection (78%) was obtained at the lowest ZnO concentration; that showed 11% increase compared with pure PEI with Na_2SO_4 rejection 59%. After

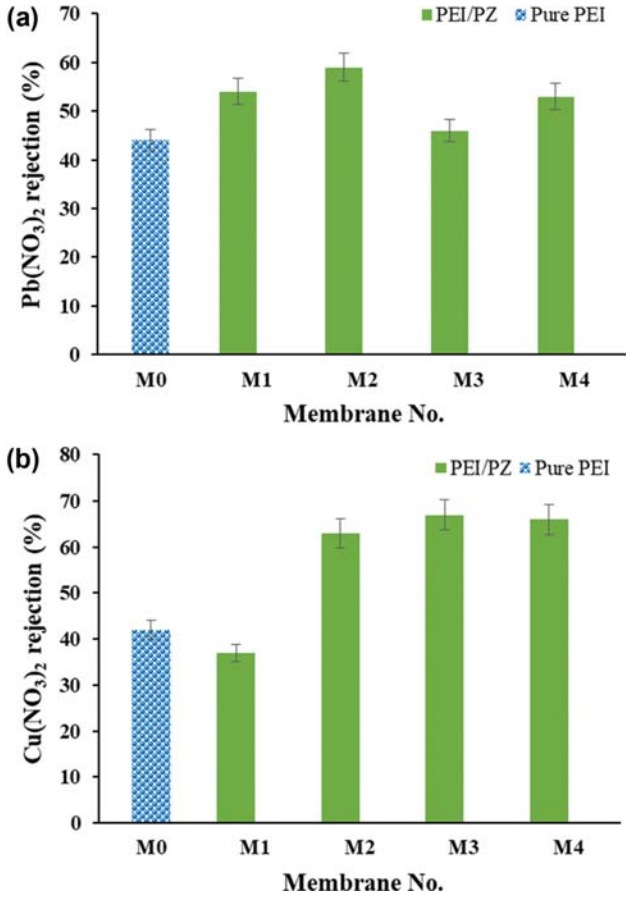

Fig. 9. The (a) $Pb(NO_3)_2$ and (b) $Cu(NO_3)_2$ rejections for prepared membranes with different concentration of PZ.

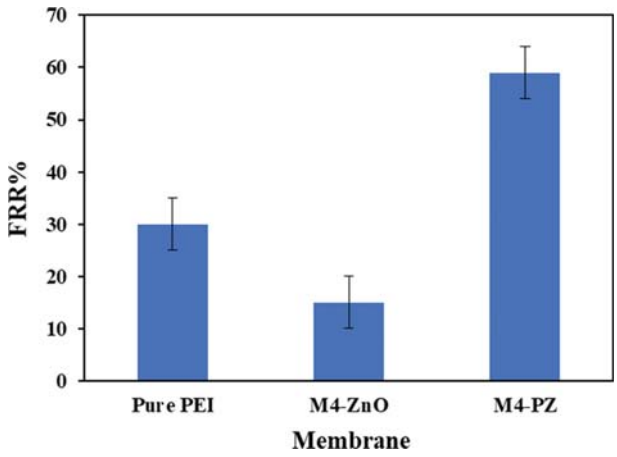

Fig. 10. The flux recovery ratio (FRR %) of pure PEI, M4-ZnO and M4-PZ in 1 wt% nanoparticles.

that, the rejection rate decreased at a high concentration of ZnO nanoparticles. However, the membrane porosity increased compared with pristine membrane according to Table 2. But the mean pore size of membranes decreased with increasing ZnO nanoparticles. The results of the mean pore size of membranes are shown in Table 2. Na_2SO_4 rejection decreased in M4 due to agglomeration of nanoparticles on the membrane and decreasing nanoparticle dispersity [38,47].

Metal aqueous solutions of $Pb(NO_3)_2$ and $Cu(NO_3)_2$ were prepared with a concentration of 500 mg/L for the examination of heavy metal ions separation. The result of metal ion rejection is shown in Figs. 9(a) and (b). POSS is a good adsorbent for heavy metals according to previous studies [18,48,49]. Therefore, PZ nanoparticles showed more separation performance of heavy metal (Pb^{2+} and Cu^{2+}) than ZnO nanoparticles. The trend of rejection rate of $Pb(NO_3)_2$ was incremental from M1 to M2, and then it decreased in M3. This process can be explained by the thickness of the selective layer and the type of channel formation. As clear in FESEM images, the thickness of the selective layer increased from M1 to M2 for both PEI/ZnO and PEI/PZ membranes. Then it decreased in M3. According to FESEM images, the M3-ZnO and M3-PZ membranes show more continuous channels in their structure compared with M2 and M4. Thus, the adsorption and transport of Pb^{2+} with ion hydrate of 4.01 Å increased and that led to reduced salt rejection [50]. In the high concentration of nanoparticles (M4), the rejection of $Pb(NO_3)_2$ increased due to the significant increasing thickness of the selective layer and the interconnecting structure of channels.

The $Cu(NO_3)_2$ rejection improved in PEI/PZ about 40% rather than pure PEI membranes and increased from 42% to 67% in M3-PZ. By incorporation of nanoparticles, the interaction between polymer and nanoparticles increased and free spaces into the membrane structure filled, which led to improving salt rejection. Against Pb^{2+} rejection, the maximum rejection of Cu^{2+} was obtained in M3-PZ. Because Cu^{2+} has higher hydrate ion (4.19 Å) than decreased ion transport. Therefore, the major mechanism for $Cu(NO_3)_2$ rejections is ion repulsion. The presence of high negative charges on the PZ particles repulses the NO_3^{2-}. Thus, the $Cu(NO_3)_2$ rejection increased with increasing nanoparticle loading and negative charges. But, in 1 wt% of PZ nanoparticles for M4-PZ occurred the agglomeration of nanoparticle and led to reducing $Cu(NO_3)_2$ rejections. Studies show that the ionic radius is the most important reason for the adsorption of Pb^{2+} and Cu^{2+}. Also, the adsorption of the small ionic radius is greater. Therefore, the adsorption of Pb^{2+} with a smaller ionic radius is more than Cu^{2+} [50-52]. The results did not exhibit a significant increase for Cu $(NO_3)_2$ rejection by PEI/ZnO nanoparticles.

4. Anti-fouling Properties of Prepared Membranes

The hydrophilicity and surface roughness of membranes, which are two important parameters for the explanation of antifouling properties, can be measured by flux recovery ratio (FRR %). As shown in Fig. 10, the highest FRR% was obtained for 1 wt% of ZnO and PZ nanoparticles. The antifouling property of PEI/ZnO membranes is very low. By introducing ZnO nanoparticles into the membrane matrix the thickness of selective layer in PEI/ZnO membranes increased significantly compared with PEI/PZ and pure PEI membranes, which led to increase membrane roughness and thus reduction of FRR% and antifouling ability. But functionalization ZnO with glycidyl POSS improved the anti-fouling property from 30% for pure membrane to 59% for M4-PZ. The presence of hydrophilic groups on the PZ nanoparticles and smoother surface membrane increased PWF after membrane fouling [53,54]. As clear

in FESEM images, the thickness of selective layer in PEI/ZnO membranes is in the range of 3.84-15.05 μm, while it is in the range of 1.38-7 μm for PEI/PZ membranes and 2.29 μm for pure PEI membrane.

CONCLUSION

Surface functionalization of zinc oxide (ZnO) nanoparticles was performed by glycidyl POSS. The synthesized nanoparticles were applied to prepare polyetherimide based-nanofiltration membranes. Generally, the incorporation of PZ nanoparticles had a significant influence on the improvement of separation performance than ZnO nanoparticles. It was revealed that M1-PZ in 0.001 wt% of PZ nanoparticles had the highest pure water flux (42.4 L/m^2h) among prepared membrane due to increasing membrane hydrophilicity and the presence of negative charges on the PZ nanoparticles that led to higher interaction with water molecules. Moreover, the highest Na_2SO_4, $Pb(NO_3)_2$ and $Cu(NO_3)_2$ rejection was obtained 83%, 59%, and 67% respectively by incorporation of PZ nanoparticles into the PEI. Donnan exclusion mechanism had the highest effect for Na_2SO_4 rejection. Pb^{2+} adsorption by PZ nanoparticles was higher than Cu^{2+} ions. Furthermore, antifouling properties improved by introducing PZ nanoparticles and FRR% reached 59% in M4-PZ.

REFERENCES

1. A. Azimi, A. Azari, M. Rezakazemi and M. Ansarpour, *ChemBioEng Reviews*, **4**, 37 (2017).
2. S. Ansari, E. Bagheripour, A. Moghadassi and S. M. Hosseini, *J. Polym. Eng.*, **37**, 61 (2017).
3. S. Tul Muntha, A. Kausar and M. Siddiq, *Polym. Plast. Technol. Eng.*, **56**, 841 (2017).
4. P. Mobarakabad, A. Moghadassi and S. Hosseini, *Desalination*, **365**, 227 (2015).
5. D. J. Miller, D. R. Dreyer, C. W. Bielawski, D. R. Paul and B. D. Freeman, *Angew. Chem. Int. Ed.*, **56**, 4662 (2017).
6. D. Rana and T. Matsuura, *Chem. Rev.*, **110**, 2448 (2010).
7. S. Bandehali, F. Parvizian, A. R. Moghadassi and S. M. Hosseini, *J. Polym. Res.*, **26**, 211 (2019).
8. A. Gholami, A. Moghadassi, S. Hosseini, S. Shabani and F. Gholami, *J. Ind. Eng. Chem.*, **20**, 1517 (2014).
9. S. S. Hosseini, A. Nazif, M. A. A. Shahmirzadi and I. Ortiz, *Sep. Purif. Technol.*, **187**, 46 (2017).
10. M. Farjami, A. Moghadassi, V. Vatanpour, S. M. Hosseini and F. Parvizian, *J. Ind. Eng. Chem.*, **72**, 144 (2018).
11. S. Bandehali, A. Kargari, A. Moghadassi, H. Saneepur and D. Ghanbari, *Asia Pacific J. Chem. Eng.*, **9**, 638 (2014).
12. S. Zinadini, S. Rostami, V. Vatanpour and E. Jalilian, *J. Membr. Sci.*, **529**, 133 (2017).
13. S. M. Hosseini, M. Afshari, A. R. Fazlali, S. Koudzari Farahani, S. Bandehali, B. Van der Bruggen and E. Bagheripour, *Chem. Eng. Res. Des.*, **147**, 390 (2019).
14. A. Pal, T. Dey, A. Singhal, R. Bindal and P. Tewari, *RSC Adv.*, **5**, 34134 (2015).
15. H. Sanaeepur, A. Ebadi Amooghin and S. Bandehali, Theoretical gas permeation models for mixed matrix membranes, LAP LAMBERT Academic Publishing (2018).
16. H. Rajabi, N. Ghaemi, S. S. Madaeni, P. Daraei, B. Astinchap, S. Zinadini and S. H. Razavizadeh, *Appl. Surf. Sci.*, **349**, 66 (2015).
17. N. Koutahzadeh, M. R. Esfahani, F. Bailey, A. Taylor and A. R. Esfahani, *J. Environ. Chem. Eng.*, **6**, 5683 (2018).
18. Y. He, Y. P. Tang and T. S. Chung, *Ind. Eng. Chem. Res.*, **55**, 12929 (2016).
19. J. Duan, E. Litwiller and I. Pinnau, *J. Membr. Sci.*, **473**, 157 (2015).
20. S. Bandehali, A. Moghadassi, F. Parvizian and S. Hosseini, *Korean J. Chem. Eng.*, **36**, 1657 (2019).
21. X. You, H. Wu, Y. Su, J. Yuan, R. Zhang, Q. Yu, M. Wu, Z. Jiang and X. Z. Cao, *J. Mater. Chem. A*, **6**, 13191 (2018).
22. M. Dalwani, J. Zheng, M. Hempenius, M. J. Raaijmakers, C. M. Doherty, A. J. Hill, M. Wessling and N. E. Benes, *J. Mater. Chem. A*, **22**, 14835 (2012).
23. X. You, T. Ma, Y. Su, H. Wu, M. Wu, H. Cai, G. Sun and Z. Jiang, *J. Membr. Sci.*, **540**, 454 (2017).
24. S. C. Chen, X. Z. Fu and T.-S. Chung, *Desalination*, **335**, 17 (2014).
25. R. S. Hebbar, A. M. Isloor, A. Ismail, S. J. Shilton, A. Obaid and H.-K. Fun, *New J. Chem.*, **39**, 6141 (2015).
26. R. S. Hebbar, A. M. Isloor and A. Ismail, *RSC Adv.*, **4**, 55773 (2014).
27. R. S. Hebbar, A. M. Isloor, K. Ananda and A. Ismail, *J. Mater. Chem. A*, **4**, 764 (2016).
28. H. Sanaeepur, A. E. Amooghin, S. Bandehali, A. Moghadassi, T. Matsuura and B. Van der Bruggen, *Prog. Polym. Sci.*, **91**, 80 (2019).
29. A. E. Amooghin, S. Mashhadikhan, H. Sanaeepur, A. Moghadassi, T. Matsuura and S. Ramakrishna, *Prog. Mater. Sci.*, **102**, 222 (2018).
30. A. Rahimpour, *Desalination*, **265**, 93 (2011).
31. Y. Mansourpanah, S. Madaeni, A. Rahimpour, A. Farhadian and A. Taheri, *J. Membr. Sci.*, **330**, 297 (2009).
32. E. Bagheripour, A. Moghadassi, S. Hosseini, B. Van der Bruggen and F. Parvizian, *J. Ind. Eng. Chem.*, **62**, 311 (2018).
33. G. Bayramoğlu, M. G. Şeker and M. Mudu, *Prog. Org. Coat.*, **101**, 510 (2016).
34. X. Wang, L. Song, H. Yang, W. Xing, B. Kandola and Y. Hu, *J. Mater. Chem. A*, **22**, 22037 (2012).
35. H. Zhang, B. Li, J. Pan, Y. Qi, J. Shen, C. Gao and B.Van der Bruggen, *J. Membr. Sci.*, **539**, 128 (2017).
36. Y. W. Chang, E. Wang, G. Shin, J. E. Han and P. T. Mather, *Polym. Adv. Technol.*, **18**, 535 (2007).
37. B. Decker, C. Hartmann-Thompson, P. I. Carver, S. E. Keinath and P. R. Santurri, *Chem. Mater.*, **22**, 942 (2009).
38. E. Bagheripour, A. Moghadassi and S. M. Hosseini, *Korean J. Chem. Eng.*, **33**, 1462 (2016).
39. H. M. Hegab and L. Zou, *J. Membr. Sci.*, **484**, 95 (2015).
40. S. Bano, A. Mahmood, S.-J. Kim and K.-H. Lee, *J. Mater. Chem. A*, **3**, 2065 (2015).
41. R. S. Hebbar, A. M. Isloor, K. Ananda, M. S. Abdullah and A. Ismail, *New J. Chem.*, **41**, 4197 (2017).
42. A. Gomathi, K. Gopalakrishnan and C. Rao, *Mater. Res. Bull.*, **45**, 1894 (2010).
43. W. L. Xu, C. Fang, F. Zhou, Z. Song, Q. Liu, R. Qiao and M. Yu, *Nano Lett.*, **17**, 2928 (2017).
44. P. Zhang, J.-L. Gong, G.-M. Zeng, C.-H. Deng, H.-C. Yang, H.-Y. Liu and S.-Y. Huan, *Chem. Eng. J.*, **322**, 657 (2017).
45. P. Zhang, J.-L. Gong, G.-M. Zeng, B. Song, H.-Y. Liu, S.-Y. Huan

and J. Li, *Chemosphere*, **204**, 378 (2018).
46. J. Wu and P. T. Mather, *J. Macromol. Sci., Part C: Polym. Rev.*, **49**, 25 (2009).
47. E. Bagheripour, A. Moghadassi, S. Hosseini, B. Van der Bruggen and F. Parvizian, *J. Ind. Eng. Chem.*, **62**, 311 (2018).
48. K. Xie, L. Jing, W. Zhao and Y. Zhang, *J. Appl. Polym. Sci.*, **122**, 2864 (2011).
49. H.-B. He, B. Li, J.-P. Dong, Y.-Y. Lei, T.-L. Wang, Q.-W. Yu, Y.-Q. Feng and Y.-B. Sun, *ACS Appl. Mater. Interfaces*, **5**, 8058 (2013).
50. S. B. Chen, Y. B. Ma, L. Chen and K. Xian, *Geochem. J.*, **44**, 233 (2010).
51. D. J. Hillel, Environmental soil physics, Academic Press, San Diego (1998).
52. D. C. Ko, C. W. Cheung, K. K. Choy, J. F. Porter and G. McKay, *Chemosphere*, **54**, 273 (2004).
53. S. Madaeni, S. Zinadini and V. Vatanpour, *Sep. Purif. Technol.*, **111**, 98 (2013).
54. L. Feng, Z. Zhang, Z. Mai, Y. Ma, B. Liu, L. Jiang and D. Zhu, *Angew. Chem. Int. Ed.*, **116**, 2046 (2004).